Boundary-Layer Meteorol (2007) 122:655–681
DOI 10.1007/s10546-006-9122-0

ORIGINAL PAPER

Modelling of concentration fluctuations in canopy turbulence

M. Cassiani · A. Radicchi · J. D. Albertson

Received: 31 October 2005 / Accepted: 1 August 2006 /
Published online: 29 November 2006

Abstract The knowledge of the concentration probability density function (pdf) is of importance in a number of practical applications, and a Lagrangian stochastic (LS) pdf model has been developed to predict statistics and concentration pdf generated by continuous releases of non-reactive and reactive substances in canopy generated turbulence. Turbulent dispersion is modelled using a LS model including the effects of wind shear and along-wind turbulence. The dissipation of concentration fluctuations associated with turbulence and molecular diffusivity is simulated by an Interaction by Exchange with the Conditional Mean (IECM) micromixing model. A general procedure to obtain the micromixing time scale needed in the IECM model useful in non-homogeneous conditions and for single and multiple scalar sources has been developed. An efficient algorithm based on a nested grid approach with particle splitting, merging techniques and time averaging has been used, thus allowing the calculation for cases of practical interest. The model has been tested against wind-tunnel experiments of single line and multiple line releases in a canopy layer. The approach accounted for chemical reactions in a straightforward manner with no closure assumptions, but here the validation is limited to non-reacting scalars.

Keywords Chemical reaction · Concentration moments · Lagrangian stochastic particle model · Micromixing model · Probability density function · Turbulent dispersion

M. Cassiani (✉) · J. D. Albertson
Department of Civil and Environmental Engineering, Duke University, 121 Hudson Hall, Box 90287, Durham, NC 27708, USA
e-mail: massimo.cassiani@duke.edu

A. Radicchi
Facoltà di Scienze Ambientali, Università di Urbino "Carlo Bo", 61029 Urbino, Italy

1 Introduction

The dispersion in a canopy layer is a very important process since it is of interest for both urban and agricultural–forest applications. Most of the research in this field has been devoted to understanding the behaviour of the mean concentration of natural and anthropogenic substances emitted into or by the canopy (e.g., Baldocchi 1992). The modelling of the evolution of the mean concentration field of a non-reactive substance inside and above a homogenous canopy layer is relatively well understood (e.g., Coppin et al. 1986, Flesch and Wilson 1992), while the prediction of higher concentration moments, i.e. the modelling of the fluctuating behaviour of the scalar field, is an open question. Knowledge of the concentration fluctuations is often required in many cases of interest in both agricultural–forest meteorology and urban meteorology. This is the case, for example, in olfactory research (Vickers et al. 2001), the chemistry of naturally emitted volatile organic compounds (VOC), as for example isoprene, anthropogenic VOC, ozone and NO_x (see, e.g., Brown and Bilger 1998a,b, Meeder and Nieuwstadt 2000, Patton et al. 2001, Brown and Woodfield 2004, Vilà-Guerau de Arellano et al. 2004, Garmory et al. 2006, Sawford 2006) and the modelling of accidental or intentional releases of toxic, flammable and explosive materials (e.g., Griffith and Megson 1984, Wilson 1995, Hilderman et al. 1999, Yee 2001).

Since its early use (Dopazo and O'Brien 1974) the probability density function (pdf) approach has been extensively developed and applied to the study of complex reacting systems in the context of chemical and combustion engineering (see e.g., Dopazo et al. 1997, Pope 1985, 2000; Fox 2003). The strength of this approach is in the ability to deal exactly with chemical reactions and to reproduce the one-point pdf of the related concentration field. This means that unclosed terms do not arise in the equations due to chemical reactions. For an incompressible flow the following equation for the one-point one-time joint pdf of velocity and scalars is derived from the Navier-Stokes and the scalar transport equations (see e.g., Pope 1985)

$$\begin{aligned}
&\frac{\partial f_{\phi U}}{\partial t} + V_i \frac{\partial f_{\phi U}}{\partial x_i} - \frac{1}{\rho}\frac{\partial \langle p\rangle}{\partial x_i}\frac{\partial f_{\phi U}}{\partial V_i} + \frac{\partial}{\partial \psi_\alpha}\left[f_{\phi U} S_\alpha(\boldsymbol{\psi})\right] \\
&\quad = -\frac{\partial}{\partial V_i}\left(f_{\phi U}\left\langle \nu\nabla^2 U_i - \frac{1}{\rho}\frac{\partial p'}{\partial x_i}\middle| \mathbf{U}=\mathbf{V}, \boldsymbol{\phi}=\boldsymbol{\psi}\right\rangle\right) \\
&\qquad - \frac{\partial}{\partial \psi_\alpha}\left(f_{\phi U}\left\langle \boldsymbol{\Gamma}\nabla^2\phi_\alpha \middle| \mathbf{U}=\mathbf{V}, \boldsymbol{\phi}=\boldsymbol{\psi}\right\rangle\right). \qquad (1)
\end{aligned}$$

Angle brackets denote the ensemble average and therefore $\langle \bullet \mid \bullet \rangle$ is the conditional expectation; ν is the viscosity of the fluid, Γ is the molecular diffusivity of the scalar, ψ is the sample space variable for scalar concentration ϕ. If multiple scalars are involved ψ_α represents the concentration of the chemical species α. The effect of different molecular diffusivities will be neglected. Although a differential diffusion effect can be important this approximation is widely used to simplify the treatment of the problem and is quite applicable in high Reynolds number turbulence. $\mathbf{V}$ is the sample space variable for the velocity vector $\mathbf{U}$, and $f_{\phi U} = f(\mathbf{V},\boldsymbol{\psi};\mathbf{x},t)$ is the Eulerian joint pdf of the velocity and concentration. On the right-hand side, the first term represents the effect of viscous stresses and the fluctuating pressure gradient and the second term (conditional Laplacian) describes the dissipative effects of turbulence and molecular diffusivity on the concentration fluctuations. The terms on the left-hand side are closed as discussed in detail in Pope (2000).

Equation 1 is usually modelled through the use of a system of ordinary and stochastic differential equations. Pope (1994, 2000) and Heinz (2003) reviewed various closures and modelling techniques for the viscous stresses and pressure gradient terms in the form of Lagrangian stochastic differential equations for velocity and position of modelled fluid particles. However, if we assume that the pdf of the velocity is known (at least approximately) and that chemistry is passive (i.e. does not alter the velocity field) then the well-mixed condition of Thomson (1987) can be used to close in an exact, although not in a unique, manner (see Thomson 1987, Wilson and Flesch 1997, Sawford 1999) the viscous stresses and pressure gradient, and this is the approach we follow here.

The closure of the second term on the right-hand side of Eq. 1 is the principal modelling challenge for the transported pdf description of turbulent mixing. This term defines the shape of the concentration pdf, and its closure is usually referred to as the micromixing model. In Lagrangian stochastic modelling a micromixing model describes the evolution of the concentration pdf using an equation for the concentration carried by each modelled particle in the domain. Micromixing models are heuristic and they are built to ensure the presence of desirable properties as discussed, e.g., in Cassiani et al. (2005a). We stress here that we are referring to modelled fluid particles not true fluid particles; the equivalence between the modelled system and realty is only in a statistical sense and limited to a one-point pdf. Therefore, a pdf model includes a set of equations for the velocity, position and concentration of each modelled fluid particle.

The micromixing model considered here is referred to as the Interaction by Exchange with the Conditional Mean (IECM), and has the desirable property of leaving unaltered the mean concentration field since it ensures that the mixing model and the velocity field are uncorrelated (see Fox 1996, Pope 1998, Sawford 2004, Cassiani et al. 2005a). In this model, the concentration relaxes to the local mean concentration conditioned over the velocity,

$$\left\langle \Gamma \nabla^2 \phi_\alpha \middle| \mathbf{U} = \mathbf{V}, \boldsymbol{\phi} = \boldsymbol{\psi} \right\rangle = -\frac{1}{t_\mathrm{m}} \left(\psi_\alpha - \langle \phi_\alpha \, | \mathbf{U} = \mathbf{V} \rangle \right), \tag{2}$$

and reflects the concept that the ultimate action of mixing is to homogenize the concentration field, thus dissipating the fluctuations. In general, the relaxation towards a conditional mean allows us to better respect the desirable properties of localness (see Pope 1998, Subramaniam and Pope 1998), i.e. particles that interact with each other should have similar position, velocity and concentration. Apart from the model itself one of the main problems dealing with the pdf approach is the specification of an appropriate micromixing time scale t_m. As can be seen, t_m defines the rate of relaxation of the concentration towards the local mean and it can be shown to be related to the dissipation time scale of concentration variance, i.e. $t_\mathrm{m} \approx \tau_\phi \equiv 2\sigma_\phi^2/\varepsilon_\phi$, where σ_ϕ^2 is the scalar concentration variance and $\varepsilon_\phi \equiv 2\Gamma \left\langle \frac{\partial \phi}{x_i} \frac{\partial \phi}{x_i} \right\rangle$ is the scalar dissipation rate (see e.g., Cassiani et al. 2005a).

Micromixing models, coupled with the LS approach, are relatively easy to apply and have been proven to be a valuable tool in evaluating concentration fluctuations for atmospheric application in non-homogeneous conditions. Recently the IECM approach has been applied to dispersion from a point source in the neutral boundary layer (Cassiani et al. 2005a), to dispersion from point and line sources in the convective boundary layer (CBL) (Cassiani et al. 2005b, Luhar and Sawford 2005a) and to

dispersion from an extensive continuous area source both in a canopy layer (Cassiani et al. 2005c) and in a CBL (Luhar and Sawford 2005b). Luhar and Sawford (2005a, b) used a pre-computed mean concentration field thus inhibiting the direct treatment of the chemistry by the model, while the approach of Cassiani et al. (2005a, b, c) allows the direct treatment of chemistry.

However, all these models are limited to single sources and are based on the use of Taylor's frozen turbulence hypothesis to reduce the dimensionality of the problem and, therefore, the computational requirements. Here, we relax these restrictions to allow the use of IECM for situations where the mean shear and along-wind turbulence are fundamental, as in the case of dispersion from localized sources in a canopy layer. We also extend the model for the micromixing time scale proposed in Cassiani et al. (2005a) to allow for the consideration of multiple sources.

In Sect. 2 the set of modelling equations are presented, and in Sect. 3 the numerical methods are discussed. In Sect. 4 the model for the micromixing time scale is presented, and in Sect. 5 the simulation results are compared with experimental data.

2 Model formulation

Starting with the modelling hypothesis of the joint Markovian velocity and position of fluid particles (see Monin and Yaglom 1975, p. 369; Thomson 1987), we solve the following system of stochastic and deterministic differential equations,

$$\mathrm{d}u_i^* = a_i(\mathbf{X}^*, \mathbf{u}^*, t)\mathrm{d}t + b_{ij}(\mathbf{X}^*, t)\mathrm{d}\zeta_j, \tag{3}$$

$$\mathrm{d}X_i^* = \left(u_i^* + \left\langle U_i^* \right\rangle\right)\mathrm{d}t, \tag{4}$$

$$\mathrm{d}\phi_\alpha^* = \varphi_\alpha(\phi_\alpha^*, \mathbf{X}^*, \mathbf{u}^*, t)\mathrm{d}t + S_\alpha(\boldsymbol{\phi}^*, \mathbf{X}^*, t)\mathrm{d}t. \tag{5}$$

From here we follow the notation of Pope (1985, 1998) indicating modelled quantities with the asterisk. The velocity field is decomposed as $\mathbf{U} = \langle \mathbf{U} \rangle + \mathbf{u}$, so that $\mathbf{u}^*$ and $\langle \mathbf{U}^* \rangle$ are the modelled fluctuating and mean particle velocities, respectively and $\mathbf{X}^*$ is the position vector. We note that the form of Eqs. 3 and 4 for the particle velocity and position is that proposed by Wilson and Flesch (1997). Further, $\mathbf{c}^*$ is the concentration associated with the particle, and $\mathrm{d}\zeta_j$ indicates a vector of independent Wiener processes with zero mean and variance dt (see Gardiner 1983).

The term φ_α is the micromixing model, Eq. 2, of the chemical species α. With the notation introduced in this paragraph we have,

$$\varphi_\alpha = -\frac{1}{t_\mathrm{m}}\left(\psi_\alpha - \left\langle \phi_\alpha^* \left| \mathbf{u}^* = \mathbf{v}, \mathbf{X}^* = \mathbf{x} \right.\right\rangle\right). \tag{6}$$

The parameterization for the micromixing time scale will be explained in Sect. 4. The source term includes both chemical reaction and emission from the source. Because the scalar is passive, the velocity is independent of the concentration field. The deterministic form of Eq. 5 simplifies the treatment but introduces some shortcomings as discussed in Cassiani et al. (2005a). A general discussion of this equation can be found in Pope (1985) and Fox (2003).

As is customary the diffusion coefficient b_{ij} is obtained by imposing consistency with the Kolmogorov similarity theory for the Lagrangian structure function (Monin

and Yaglom 1975) in the inertial sub range, i.e. $b_{ij} = \delta_{ij} (C_0 \varepsilon)^{1/2}$, where δ_{ij} is the Kronecker delta, C_0 is the Kolmogorov constant and ε is the mean dissipation rate of turbulent kinetic energy. The drift coefficient a_i is obtained by ensuring the fulfilment of the well-mixed condition (Thomson 1987), namely the consistency of Eqs. 3 and 4 with an assumed pdf of the Eulerian fluctuating velocity $f_u^*(\mathbf{v}; \mathbf{x}, t)$. Here we assume a Gaussian inhomogeneous turbulent field inside and above the canopy, a choice that has proven adequate in simulating dispersion in a canopy layer (Flesch and Wilson 1992, Cassiani et al. 2005c). With this choice, and assuming the principal axis aligned with the mean wind and the third axis oriented in the vertical direction, we have the following formulation for the pdf $f_u^* = g_{u_1 u_3} g_{u_2}$ with

$$g_{u_2} = \frac{1}{\sqrt{2\pi \left\langle u_2^2 \right\rangle}} \exp\left(-\frac{v_2^2}{2 \left\langle u_2^2 \right\rangle} \right), \tag{7a}$$

$$g_{u_1 u_3} = \frac{1}{2\pi \left(\left\langle u_1^2 \right\rangle \left\langle u_3^2 \right\rangle - \langle u_1 u_3 \rangle^2 \right)^{1/2}} \exp\left(-\frac{v_1^2 \left\langle u_3^2 \right\rangle + v_3^2 \left\langle u_1^2 \right\rangle - 2 v_1 v_3 \langle u_1 u_3 \rangle}{2 \left(\left\langle u_1^2 \right\rangle \left\langle u_3^2 \right\rangle - \langle u_1 u_3 \rangle^2 \right)} \right). \tag{7b}$$

A comment on the notation used in Eq. 7: in general the moments needed to define the velocity pdf could come from parameterization schemes or from a second-order turbulence closure model, and should be interpreted as moments of the modelled variables, for example we could use $\left\langle u_1^* u_3^* \right\rangle$ instead of $\langle u_1 u_3 \rangle$. However, when the velocity moments are taken directly from the interpolation of the experimental data that we are simulating, they can be interpreted as true fluid velocity moments, i.e. $\left\langle u_1^* u_3^* \right\rangle = \langle u_1 u_3 \rangle$ (given the uncertainty in the experiments and interpolation). Since this is our case we use this simpler notation.

Therefore in stationary conditions the drift coefficients for each component of the velocity vector can be obtained as discussed extensively in Thomson (1987), Wilson and Flesch (1997) and Rodean (1996) and here reported in the Appendix.

We briefly note that the ensemble of solutions of the system (3), (4), (5) correspond to that of a system containing stochastic equations for the full particle velocity instead of the fluctuating component if the Thomson's (1987) solution for Gaussian turbulence is used. In fact the following equivalence,

$$\begin{aligned} \frac{\partial f_{\phi u}^*}{\partial t} + \frac{\partial}{\partial x_i} \left[(v_i + \langle U_i \rangle) f_{\phi u}^* \right] = & \frac{\partial f_{\phi U}^*}{\partial t} + \frac{\partial}{\partial x_i} \left[(v_i + \langle U_i \rangle) f_{\phi U}^* \right] \\ & + \frac{\partial f_{\phi U}^*}{\partial V_i} \left(\frac{\partial \langle U_i \rangle}{\partial t} + (v_i + \langle U_i \rangle) \frac{\partial \langle U_i \rangle}{\partial x_j} \right), \end{aligned} \tag{8}$$

shows that the last term on the right-hand side $\left(\partial \langle U_i \rangle / \partial t + (v_i + \langle U_i \rangle) \, \partial \langle U_i \rangle / \partial x_j \right)$ is exactly what we miss comparing Φ_i / f_u to the corresponding coefficient obtained for the full particle velocity, as discussed in Sawford (1999). This shows the equivalence of the two formulations once the mean velocity field is known.

Re-writing the system of Eqs. 3–5, in the form of a Fokker–Planck equation for the joint pdf of the fluctuating velocity and concentration $f_{\phi u}^*$,

$$\begin{aligned} \frac{\partial f_{\phi u}^*}{\partial t} + \frac{\partial}{\partial x_i} \left[(v_i + \langle U_i \rangle) f_{\phi u}^* \right] = & -\frac{\partial}{\partial \psi_\alpha} \left(S_\alpha f_{\phi u} \right) - \frac{\partial}{\partial v_i} \left(a_i f_{\phi u}^* \right) + \frac{\partial^2}{\partial v_i \partial v_j} \left(B_{ij} f_{\phi u}^* \right) \\ & - \frac{\partial}{\partial \psi} \left(\varphi f_{\phi u}^* \right), \end{aligned} \tag{9}$$

and comparing Eqs. 1 and 9 we see that the coefficients a_i and b_{ij} jointly model the conditional viscous stress and fluctuating pressure gradients. Since in this approach the mean velocity field is known we avoid the need to solve a Poisson equation for the mean pressure field.

3 Numerical algorithm

We will now briefly explain the methods used to extract meaningful concentration statistics from the solution of Eqs. 3–5. Full details of the algorithm, including the analysis of the convergence to a significant solution and the analysis of the statistical and discretization errors, can be found in Cassiani et al. (2006).

We recall that a significant ensemble of solutions of Eqs. 3–5 corresponds to a Monte Carlo solution of the Fokker–Plank Equation (9). In general, pdf modelling requires intensive computations both in terms of CPU time and memory requirement because the equations of motion of a sample of all fluid particles, i.e. particles uniformly distributed over the domain, have to be solved (see e.g., Fox 2003); chemical reactions can be included in closed-form only if the equations are solved in parallel. Considering a computational domain of a given size the computation is longer the smaller the source size because the grid should be refined in order to provide details of the concentration field around the source, and as a consequence a large number of particles needs to be simulated in order to have meaningful statistics at each grid point. This is a significant problem in atmospheric dispersion applications because usually the source size is very small compared to the domain relevant to the dispersion.

In this section we describe an efficient and original computational method based on a block structured (nested) grid approach coupled with a technique of particle splitting and erasing as needed to maintain a statistically constant mean particle number in the smaller and larger cells. This approach coupled with different particle masses (greater in the larger cells and smaller in the smaller cells) is able to maintain a statistically constant mass density in the domain, and this is the actual prerequisite for meaningful calculations in an incompressible flow. Therefore for the density ρ_j of every cell we have,

$$\rho_j = \frac{\sum_{n=1}^{N_j} \mu_n}{\Delta x_1 \Delta x_2 \Delta x_3} \approx \text{const} \tag{10}$$

for $j = 1, \ldots, N_{\text{cell}}$. Here N_{cell} is the total number of cell in the physical domain, N_j is the number of particles in the jth cell, $\Delta x_1 \Delta x_2 \Delta x_3$ represents the cell volume and μ_n is the mass of the nth particle. We point out that in incompressible calculations the particle mass can be simply interpreted as a computational weight.

We also make use of time averaging to further reduce the statistical error and ensure a meaningful solution with a reduced number of particles. The use of all these techniques has been recently explored in the context of combustion engineering (Jenny et al. 2001, Li and Modest 2001) and the algorithm used here is an adaptation–optimization of their results for atmospheric application fully exploiting the use of the well-mixed condition of Thomson (1987). This optimization allows the use of the IECM micromixing modelling technique for cases of atmospheric dispersion of practical interest, even involving three-dimensional inhomogeneous flows and scalar configurations.

3.1 The grid

Knowing a priori the pdf of the velocity field the grid refinement can be related mainly to the scalar configuration, thus allowing an optimal treatment of the properties of the scalar around the source. To achieve a satisfactory resolution of the scalar field around the source while maintaining reasonable computational time and memory requirement, we adopted a block structured grid with a constant ratio of refinement between the different blocks. Figure 1 shows an example of a two-dimensional grid structure that will be used, as explained in Sect. 5, to simulate the line source experiment of Legg et al. (1986). The source spans the crosswind direction (i.e. direction 2) and is located in the middle of the most refined cells. We note that the scalar field in this experiment has only two dimensions of non-homogeneity such that we can reduce the problem to a two-dimensional one. We give full details of the experiment in Sect. 5.

We indicate with $l = 1, \ldots, N_g$ the levels of the block structure, with N_g characterizing the most refined block. The ratio between the cell sizes (line, area, volume) of two adjacent levels is R^d with R being the ratio between the size of one side of a cell at level l and the side of a cell at level $l + 1$, i.e.

$$R = \Delta x_1|_l / \Delta x_1|_{l+1} \tag{11}$$

with d being the dimensionality of the grid. For example in Fig. 1 the ratio is $R = 2$ and the dimensionality is $d = 2$.

The IECM model requires the localization of particles even in velocity space, and therefore the grid must also cover the velocity space. For example in this work we show results in two dimensions, and this means that the grid is actually four dimensional. The velocity space has been discretized with nine velocity classes for each velocity component, where each class covers approximately the same area under the velocity pdf. Extensive tests have been conducted to evaluate the effect of the number of velocity classes on the simulation results and a full explanation is given in Cassiani et al. (2006).

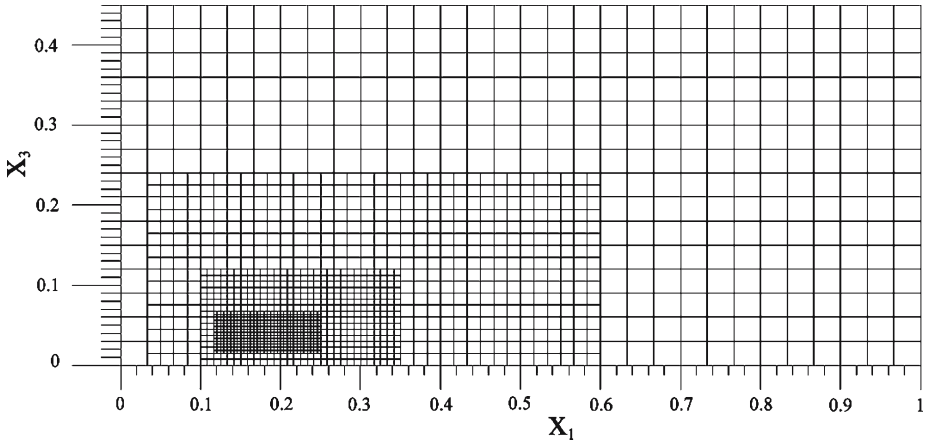

Fig. 1 Example of the block-structure grid used to simulate the single-line source experiment of Legg et al. (1986). Here x_1 is the along-wind coordinate in the computational domain and x_3 is the elevation above ground, both in metres. The source is located at $x_1 = 0.14$ m and $x_3 = 0.051$ m, within the most refined grid resolution

3.2 Particle splitting–erasing

To maintain a constant statistical error particle splitting–erasing (SE) is adopted to ensure that we have approximately the same number of particles in each cell irrespective of the cell size. To maintain a constant density each particle has a mass μ_n that depends on the size of the cell within which it is located: the smaller the cell the smaller is μ_n. Therefore the mass is a function of the block level l in which the particle is located,

$$\mu_n = \left(\frac{1}{R^d}\right)^{l-1}. \tag{12}$$

The SE algorithm is composed of two parts:

Particle splitting: when a particle of mass μ_n starting from a cell at the grid level $l-1$ arrives in a cell at the grid level l, it is split into R^d "children" particles each of mass $\mu_i = \frac{1}{R^d}\mu_n$, with $i = n, N_\mathrm{p}+1, \ldots, N_\mathrm{p}+R^d-1$. Here N_p is the total number of particles before the splitting. These "children" particles inherit all the properties of the "mother" particle $(\mathbf{u}^*, \mathbf{X}^*, \boldsymbol{\phi}^*)$ except clearly the mass. For successive timesteps these particles move independently. Figure 2 shows a sketch of the particle splitting for the two-dimensional grid previously shown in Fig. 1.

Particle erasing: when a particle of mass μ_n arising from a cell at grid level l arrives in a cell at grid level $l-1$ it has a probability $P = 1/R^d$ of surviving and probability $q = 1-P$ of being erased. The mass of any surviving particle becomes R^d times the mass of an original particle.

We point out that the SE procedure is executed at the time of crossing the border of adjacent blocks; the influence of the SE procedure on the model results has been investigated in Cassiani et al. (2006). It is worth noting that with this structured approach we avoid any computationally expensive a posteriori treatments of the particle mass. For example there is no need for any mass sorting algorithm, which is

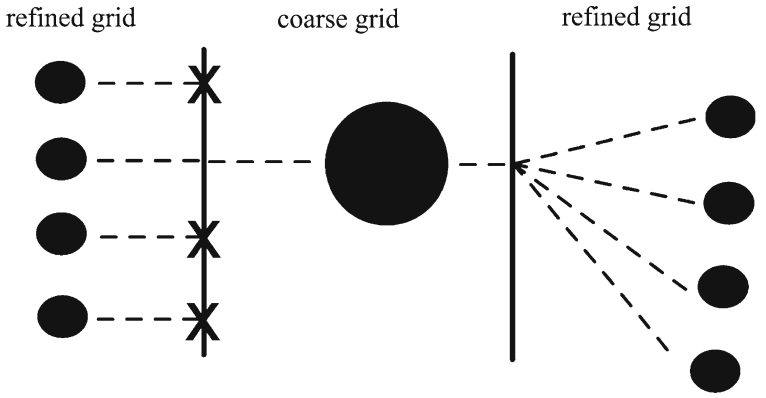

Fig. 2 Sketch of the particle erasing and splitting for a two-dimensional grid with refinement factor $R = 2$. Particle erasing procedure (left) with probability 3/4 when entering a coarser grid block: the surviving particle retains its characteristics while the computational weight is increased. Particle splitting (right) when entering a refined grid block: the new particles have a computational weight of 1/4 of the original particle

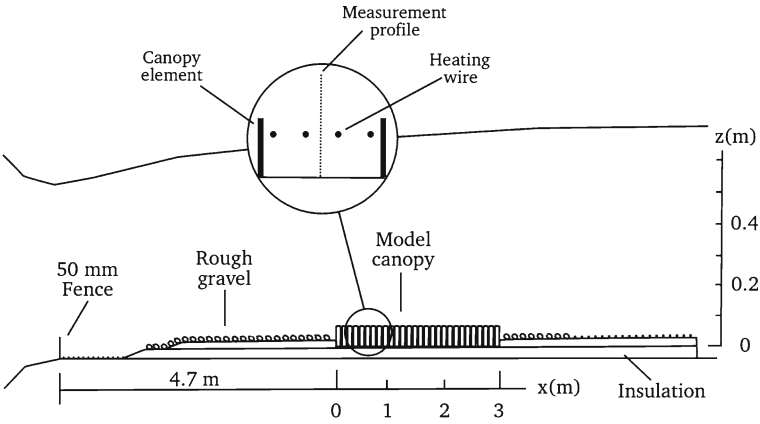

Fig. 3 Wind-tunnel configuration in Raupach et al. (1986). Here $x = x_1$ and $z = x_3$

usually used to ensure constant density in unstructured grid (see e.g., Li and Modest 2001).

3.3 Computation of statistics and numerical integration of the equations

The initial particle velocity is extracted from the local velocity pdf, and the particle positions are initially distributed in the physical domain with a uniform random distribution. The scalar value in each particle position depends on the source scalar distribution. Once the particle properties are initialized the computation starts.

The system of Eqs. 3–5 is discretized with a simple Euler scheme. The effects of the micromixing model, sources and chemical reactions on particle composition are separated following the method of the fractional step. This decoupling of chemistry and mixing allows the use of optimal methods for the solution of the system of differential equations for chemical reactions (see e.g., Fox 2003).

Particles are subject to a global timestep and to an individual smaller timestep. The global timestep Δt_{g} is the result of a sum of many individual timesteps, and is the same for all the particles in the domain and therefore synchronizes the particles. The conditional mean field used in the IECM model is updated at the end of each global timestep. The individual timestep is used to update the particle position velocity and concentration. The constraint in the choice of the global timestep is

$$\frac{\Delta t_{\mathrm{g}} \max\left(\langle u_1 \rangle\right)}{\Delta x_1|_{l=1}} < 1 \tag{13}$$

to ensure that the mean field cannot vary in a significant manner between two different timesteps. We recall that $l = 1$ refers to the first level of the grid structure.

The individual timestep is more restricting and is limited by the following conditions

$$\max\left(\frac{\Delta t \langle u_1 \rangle}{\Delta x_1|_l}, \frac{\Delta t \sigma_{u_i}}{\Delta x_i|_l}, \frac{\Delta t}{T_{\mathrm{L}}}, \frac{\Delta t}{t_{\mathrm{m}}}\right) \ll 1 \tag{14}$$

implying that the timestep is chosen to ensure that the greatest of these ratios is much less than unity; typically we chose the greatest ratio to be 0.03. Here each quantity is evaluated at the particle position. $\Delta x_i|_l$ and t_m are cell dependent while $\langle u_1 \rangle$, σ_{u_i} and

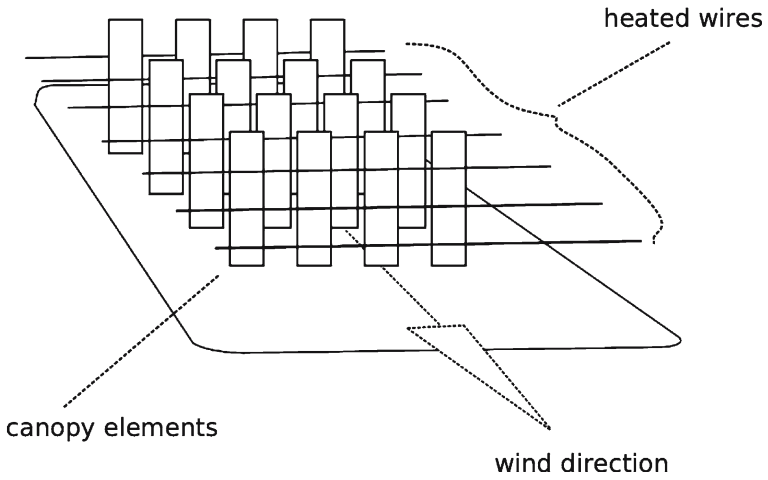

Fig. 4 Sketch of the source configuration in the experiment of Coppin et al. (1986). The along-wind direction corresponds to x_1 while the crosswind coordinate (spanned by the heated wires) corresponds to x_2

Table 1 Flow and source details of the wind-tunnel experiments

Flow details, Raupach et al. (1986)	
Canopy height	$h_c = 60\,\text{mm}$
Friction velocity	$u_* = 1.03\,\text{m s}^{-1}$
Roughness length	$z_0 = 8.7\,\text{mm}$
Boundary Layer depth	$\delta = 540\,\text{mm}$
Single line source details, Legg et al. (1986)	
Source height	$h_s = 51\,\text{mm}$
Wire diameter	0.9 mm
Source strength	$Q_s = 60\text{–}350\,\text{W m}^{-1}$
Temperature scale	$\theta_* = Q_s/(\rho_a C_p h_s u_s)$
Multiple line sources details, Coppin et al. (1986)	
Source height	$h_s = 48\,\text{mm}$
Wire diameter	0.25 mm
Spacing between wires	22 mm
Sources downwind extension	2.12 m
Source strength	$Q_s = 275\,\text{W m}^{-2}$
Temperature scale	$Q_* = Q_s/(\rho_a C_p u_*)$

T_L (Lagrangian integral time scale) depend continuously on the particle position. For a full explanation of the effect of the timestep size on the results see Cassiani et al. (2006).

The grid is used to compute cell-averaged quantities, which are estimators of ensemble-averaged quantities (see Pope 1985; 2000 and references therein), although each quantity is also time averaged over the duration of a global timestep. Thus, for example, the cell-averaged mean concentration for the jth cell is defined,

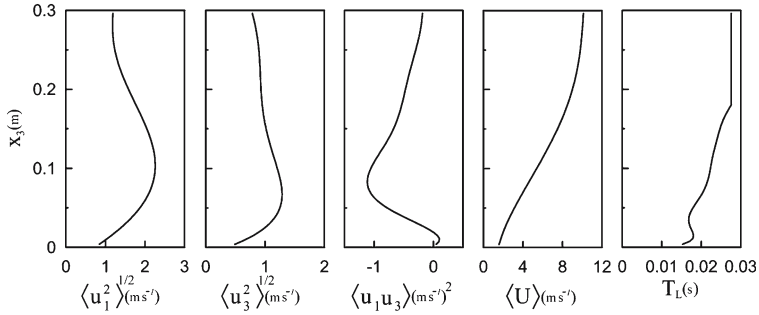

Fig. 5 Stationary vertical profile obtained from a polynomial interpolation of the data reported in Raupach et al. (1986), Legg et al. (1986) and Raupach et al. (1987). Variance of the along-wind component of velocity fluctuation, $\langle u_1^2 \rangle$; variance of the vertical component of velocity fluctuation, $\langle u_3^2 \rangle$; covariance, $\langle u_1 u_3 \rangle$; mean wind, $\langle U \rangle$; Lagrangian time scale, T_L

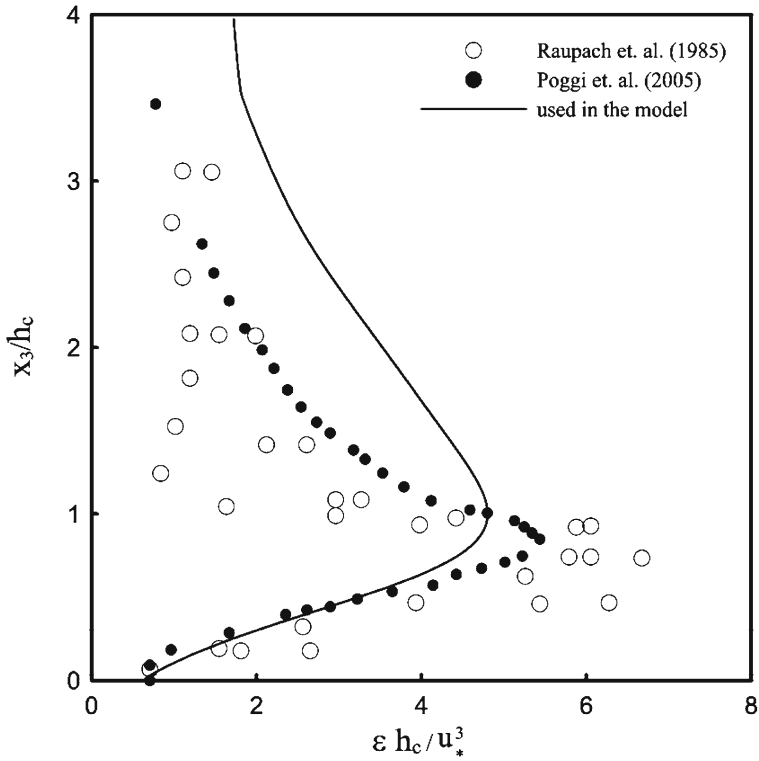

Fig. 6 Mean dissipation profile resulting from the relation, $T_L = 2\langle u_3^2 \rangle / C_0 \varepsilon$ (line) and the values estimated using three different methods by Raupach et al. (1986). The estimates from Poggi et al. (2006) in a similar canopy are included for comparison

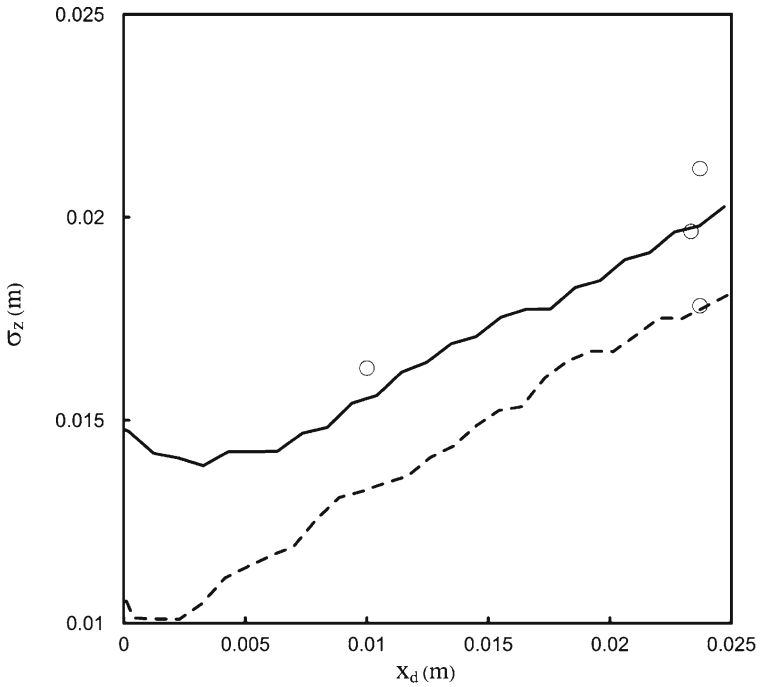

Fig. 7 Close-to-the-source vertical standard deviation of the absolute dispersion (σ_z) computed by the model for two different source sizes; 0.9 mm, dashed line; 4.5 mm continuous line. The opens symbols are the measurements from Legg et al. (1986)

$$\langle \phi^* \rangle_j = \frac{\sum_{n=1}^{N_\mathrm{p}} \left(\hat{k}_j(\mathbf{X}^*) \phi^* \mu \Delta t \right)_n}{\sum_{n=1}^{N_\mathrm{p}} \left(\hat{k}_j(\mathbf{X}^*) \mu \Delta t \right)_n} \tag{15}$$

where N_p is the total number of particles and the subscript n refers to the properties of the nth particle. Here the kernel estimator $\hat{k}$ is simply

$$\hat{k}_j(\mathbf{X}^*) = 1 \quad \text{if } \mathbf{x}_j \leq \mathbf{X}^* < \mathbf{x}_j + \Delta \mathbf{x}_j, \tag{16a}$$

$$\hat{k}_j(\mathbf{X}^*) = 0 \quad \text{otherwise.} \tag{16b}$$

Here $\mathbf{x}_j$ and $\mathbf{x}_j + \Delta \mathbf{x}_j$ represent the boundaries of the jth cell in the three-dimensional physical space and should not be confused with the indicial notation for the coordinate system. Equation 16 means simply that particles contribute to the averaged values in a cell if they are inside the cell. However, other kernel definitions are possible (see e.g., Fox 2003).

Equation 15 can be formally extended to represent velocity conditioned averages. For example the jth cell mean concentration conditioned on the kth velocity class is,

$$\langle \phi^* \rangle_{j,k} = \frac{\sum_{n=1}^{N_\mathrm{p}} \left(\hat{\hat{k}}_{j,k}(\mathbf{X}^*, \mathbf{u}^*) \phi^* \mu \Delta t \right)_n}{\sum_{n=1}^{N_\mathrm{p}} \left(\hat{\hat{k}}_{j,k}(\mathbf{X}^*, \mathbf{u}^*) \mu \Delta t \right)_n} \tag{17}$$

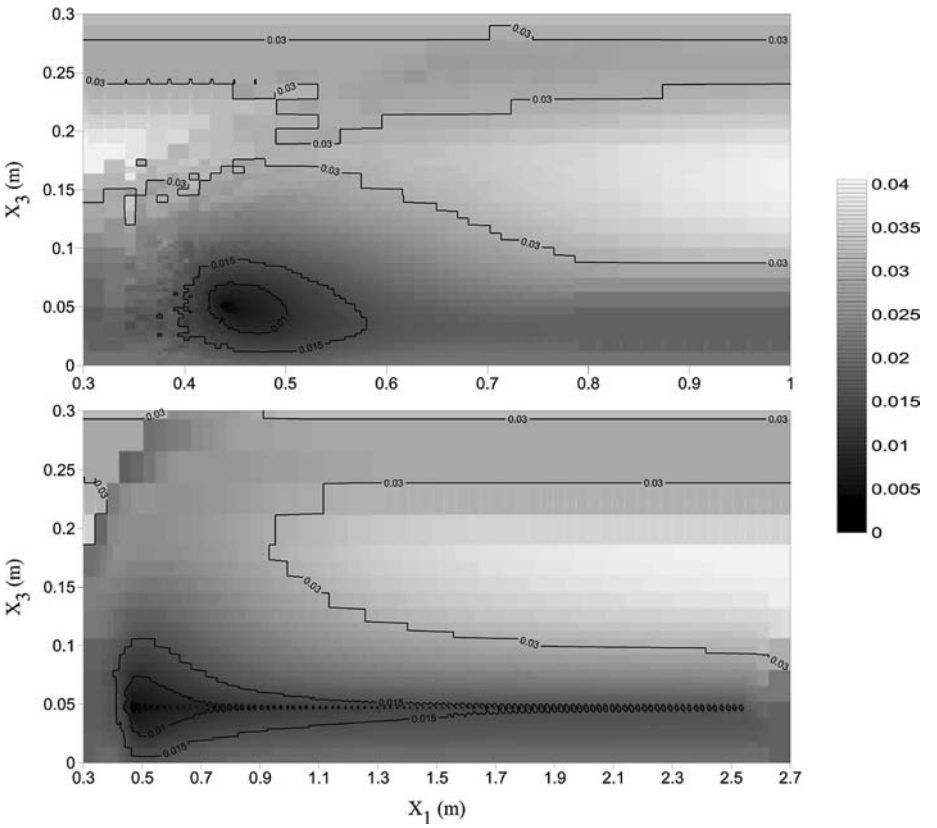

Fig. 8 Comparison of the micromixing time scale (t_{m}) computed by the model for a single-line source (**a**) and multiple-line sources (**b**); x_1 is the along-wind coordinate of the computational domain, corresponding here to the distance from the canopy boundary (see Fig. 3). x_3 is the elevation above the ground

where the kernel extends into the velocity space. It should be clear from this discussion that $\langle \phi^* \rangle_{j,k}$ is the estimator of $\langle \phi^* | \mathbf{X}^* = \mathbf{x}, \mathbf{u}^* = \mathbf{v} \rangle$.

Considering the constraints on the global timestep the above explained mean quantities should be meaningful even in non-stationary conditions, although this has yet to be tested experimentally. However, once the system reaches a stationary state we can use long time averaging to reduce the statistical error. For example, the long time-averaged mean concentration in the jth cell is,

$$\overline{\langle \phi^* \rangle_j} = \frac{\sum_{n=1}^{N_{\mathrm{t}}} \left(\langle \phi^* \rangle_j \, \Delta t^{\mathrm{g}} \right)_n}{\sum_{n=1}^{N_t} \left(\Delta t^{\mathrm{g}} \right)_n} = \frac{\sum_{n=1}^{N_{\mathrm{t}}} \left(\langle \phi^* \rangle_j \right)_n}{N_t}, \tag{18}$$

where N_{t} is the number of global timesteps involved in the time averaging, which is represented with the overbar. The right equivalence in Eq. 18 follows since the global timestep is constant.

All the model results presented here for the scalar field involve this time-averaging operation; therefore, for simplicity, we will use only $\langle \bullet \rangle$ to indicate the double averaging operation when modelled scalar statistics are considered.

4 The micromixing time scale

We discuss now a semi-empirical formulation for the micromixing time scale to be used in the micromixing model, and begin with a short discussion of the time-scale parameterization for homogeneous isotropic turbulence (see also Cassiani et al. 2005a, for a comprehensive discussion) and afterward we present the extension to inhomogeneous turbulence and multiple sources.

Following Sawford (2004) we assume $t_m = \gamma t_r = \gamma \sigma_r / \sigma_{ur}$ at short and medium distances from the source, where γ is an empirical constant to be evaluated after comparison with experiments and dependent on the source geometry, σ_r is the mean relative plume spread (i.e. the spread relative to centre of mass) and $\sigma_{ur} = \langle u_r^2 \rangle^{1/2}$ is the standard deviation of the relative velocity fluctuations where u_r indicates the difference between a turbulent velocity component and the corresponding velocity component of an instantaneous centre-of-mass of a cluster of particles.

σ_{ur} is modelled using the following formulation (Franzese 2003, Cassiani et al. 2005a):

$$\sigma_{ur}^2 = \sigma^2 \left(\frac{\sigma_r}{L} \right)^{2/3} \tag{19}$$

where σ^2 is the variance of each turbulent velocity component and is the same in any direction because of isotropy, $L \equiv \left(3\sigma^2/2\right)^{3/2} \varepsilon^{-1} = k^{3/2}\varepsilon^{-1}$ is a characteristic length scale of the most energetic eddies σ_r is parameterized as

$$\sigma_r^2 = \frac{d_r^2}{1 + (d_r^2 - \sigma_0^2)/(\sigma_0^2 + 2\sigma^2 T_L t)}, \tag{20}$$

where

$$\mathrm{d}_r^2 = C_r \varepsilon (t_0 + t)^3, \tag{21}$$

with $t_0 = \left[\sigma_0^2/(C_r\varepsilon)\right]^{1/3}$ being the inertial range formulation for dispersion from a finite source size (Franzese 2003), C_r is the Richardson–Obukhov constant (see Franzese and Cassiani 2006, for a comprehensive discussion of the Richardson–Obukhov constant and relative dispersion of a cluster), σ_0 is the source size and $T_L \left(= \frac{2\sigma^2}{C_0 \varepsilon}\right)$ is the Lagrangian integral time scale. The numerical value of the coefficient γ is chosen to have a satisfactory comparison with the experiments and is given below in the section of the comparison with experimental data.

4.1 Extension to the inhomogeneous condition and to multiple sources

The definition of t_m in inhomogeneous turbulence follows the scheme outlined for homogeneous isotropic turbulence, although in this case the turbulence statistics are not isotropic and not homogeneous. We will consider here the case of vertically inhomogeneous turbulence but the procedure can be easily extended to a more general case. We define a local mean velocity variance σ^2 by averaging the variances of the three components of velocity, i.e. $\sigma^2 = \left(\langle u_1^2 \rangle + \langle u_2^2 \rangle + \langle u_3^2 \rangle\right)/3$, and a space dependent t_m is then evaluated in each cell of the discretized domain.

The equation for the relative expansion in the inertial subrange, Eq. 21, is discretized as

$$d_{\mathrm{r}}^2(t+\Delta t) = d_{\mathrm{r}}^2(t) + 3C_{\mathrm{r}}\varepsilon(t_0+t)^2\,\Delta t, \tag{22}$$

and is then integrated along an ensemble of particle trajectories starting from the source location. The ensemble is instantaneously released at the source location and the trajectories are followed as soon as the particles are within the computational domain. We point out that the use of Eq. (22) in non-homogeneous, non-isotropic turbulence is an approximation. However, several experiments have provided some evidence of matching the Richardson–Obukhov law even in atmospheric turbulence (see Monin and Yaglom 1975, p. 565; Gifford 1977) thus giving some support to the use of this simple approximation.

Therefore, the dissipation $\varepsilon = \varepsilon(z)$ is calculated at each particle position and $d_{\mathrm{r}}^2(0) = \sigma_0^2$. Parameterization (20) is then used, with the height-dependent quantities σ^2 and T_{L} calculated again at the current particle position. In summary, an ensemble of values of t_{m} is pre-calculated using an ensemble of particles released from the source location, and a cell-averaged value of t_{m} is then calculated by accounting for the contribution of each particle in that cell, i.e.

$$\langle t_{\mathrm{m}}\rangle_j = \frac{\sum_{i=1}^{N_{\mathrm{t}}}\left[\sum_{n=1}^{N_{\mathrm{p}}}\left(\hat{k}_j(\mathbf{X}^*)t_{\mathrm{m}}\Delta t\right)_n\right]_i}{\sum_{i=1}^{N_{\mathrm{t}}}\left[\sum_{n=1}^{N_{\mathrm{p}}}\left(\hat{k}_j(\mathbf{X}^*)\Delta t\right)_n\right]_i}. \tag{23}$$

Here N_{t} is the number of timesteps needed so that all the particles exit the domain. This averaged value of t_{m} is then used in the discretized IECM model equation, though it should be noted that this average is different from the time average shown before. Here the number of particles contributing to the averaged value is not statistically constant in each timestep, and so the double summation selects all the particles that transit through the cell during the N_{t} timesteps.

An example of the computed micromixing time scale resulting for the line source experiments of Legg et al. (1986) is reported later in Fig. 8. In cells where no particle is present, the averaged micromixing time scale is zero. These cells, for example, are those before the source or more generally those outside of the absolute particle spread. In these cells the mean concentration of substance arriving from the source is either zero or close to zero causing a relative unimportance of the t_{m} value. However, the micromixing model should be applied even in this space, and therefore the usual equilibrium condition $t_{\mathrm{m}} = k/(\varepsilon C_\phi)$ (see e.g., Pope 2000) is imposed in these parts of the domain. C_ϕ is a proportionality constant, which, following our definition of t_{m}, is usually set to be approximately one. For clarity, we note that often in the literature a definition of t_{m} has been used that is one half of our definition, and in such a case C_ϕ results to be approximately two. This value of t_{m} can be considered as an equilibrium value allowed when the scalar field has a characteristic length scale comparable or greater than that of the velocity field and is often used in reactive calculations in the context of chemical engineering, see Cassiani et al. (2005a) for a short discussion and Fox (2003) for a comprehensive discussion. To be consistent with this choice we also impose the additional constraints that the micromixing time scale is $t_{\mathrm{m}} = k/(\varepsilon C_\phi)$ each time the averaged value (23) is larger than this equilibrium value.

The modelling extension for multiple sources of the same scalar is straightforward since we simply release particles from each source and then proceed to the averaging

in Eq. 23. In such a way we obtain a unique micromixing time scale that should be a representation of the different sources. An alternative approach could be the use of different micromixing time scales for the same scalar if this has been emitted by different sources (Luhar and Sawford 2005b). However, this introduces the need to distinguish the scalars when emitted from different sources, thus causing a great increase in the computer memory requirement. The micromixing time scale resulting from a series of 96 line sources in the Coppin et al. (1986) experiments is reported in Fig. 8 and discussed in Sect. 5.

5 Simulation of single source and multiple line sources

We use the wind-tunnel experiments described in Raupach et al. (1986), Coppin et al. (1986) and Legg et al. (1986) to test the capability of our model for releases inside a canopy. These experiments are well documented and present accurate measurements of both velocity statistics and scalar statistics up to the fourth moment. Moreover, these experiments have investigated both single source (Legg et al. 1986) and multiple source configurations (Coppin et al. 1986).

A boundary layer was developed initially over a section of roughness constructed from stones, after which the flow encountered the model canopy that extended for 3.0 m in the streamwise direction and covered the full width of the tunnel—see Fig. 3. The model canopy was an array of aluminium strips, each 10 mm wide, 1 mm thick, and 60 mm high, arranged in a regular diamond pattern with 60 mm cross-stream and 44 mm streamwise spacing. The source was a single hot wire in the Legg et al. (1986) experiment and was composed of a series of hot wires in that of Coppin et al. (1986), each wire extending across the wind-tunnel width in the crosswind direction as clarified in Fig. 4. We point out that this configuration allows us to treat the problem as two-dimensional. Some quantitative properties of the wind tunnel including both flow and source characteristics are reported in Table 1. We note here that in Coppin et al. (1986) the source was regarded as a plan source but was effectively multiple line sources as considered here. The heat generated by the sources was non-buoyant and acted as a passive tracer, as extensively discussed in the original papers, implying that we can regard the measured variation of temperature as a variation of concentration.

The velocity statistics needed to define the LS model are shown in Fig. 5. Profiles have been obtained from a polynomial interpolation of the data reported in Raupach et al. (1986) ($\langle U\rangle, \langle u_1 u_3\rangle, \langle u_3^2\rangle$), Raupach et al. (1987) ($\langle u_1^2\rangle$) and Legg et al. (1986) (T_{L}). When needed the value of $\langle u_2^2\rangle$ has been estimated from the relation $\langle u_2^2\rangle = \left(\langle u_1^2\rangle \langle u_3^2\rangle\right)^{1/2}$ as suggested by Brunet et al. (1994). We consider $T_{\mathrm{L}} = T_{u_3\mathrm{L}}$, where $T_{u_3\mathrm{L}}$ is the Lagrangian time scale for the vertical velocity, and in agreement with the literature for dispersion modelling, see e.g., the conclusion of Raupach et al. (1996). It follows that we can estimate the dissipation from the relation $T_{\mathrm{L}} = 2\langle u_3^2\rangle / C_0\varepsilon$. The exact value of the constant C_0 is still a matter of study (see e.g., Du et al. 1995; Du 1997, Reynolds 1998, Lien and D'Asaro 2002, Heinz 2003), with a range between two and seven. The lowest values are usually reserved for planetary boundary-layer turbulence and decaying grid turbulence while the upper limit is usually obtained in direct numerical simulation (DNS) of homogenous isotropic turbulence. In Cassiani et al. (2005a) a value of $C_0 = 5$ was used to obtain good agreement with mean concentration data obtained by Fackrell and Robins (1982). Here the satisfactory agreement

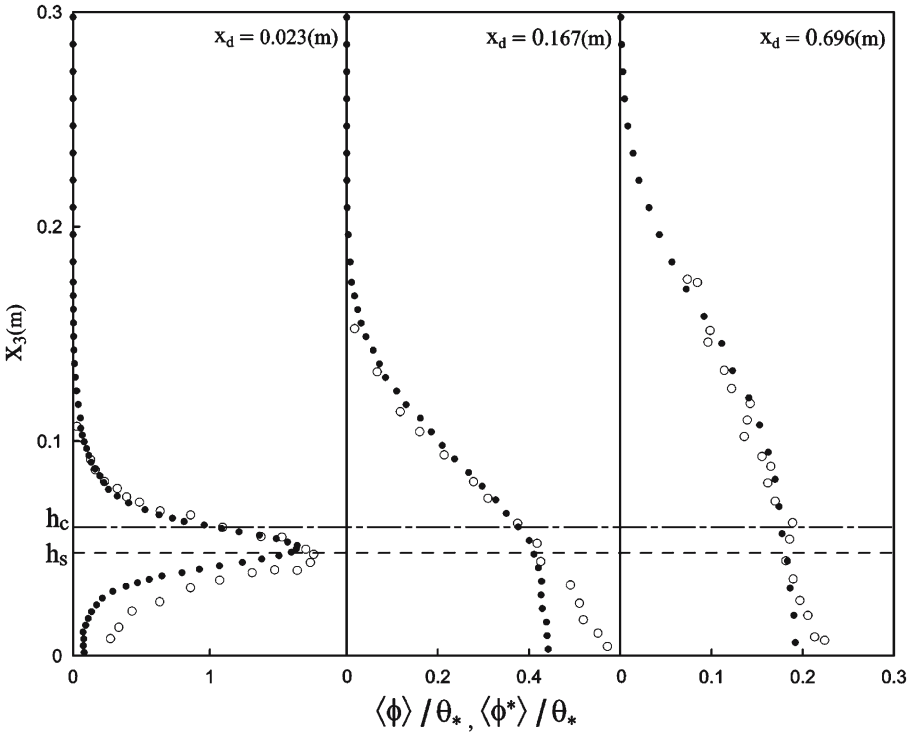

Fig. 9 Measured ($\langle\phi\rangle$, ○) and modelled ($\langle\phi^*\rangle$, ●) mean temperature normalized with the temperature scale θ_* (see Table 1); Single-line source experiments of Legg et al. (1986). $h_c = 0.06$ m is the canopy height; $h_s = 0.048$ m is the source height; x_d is the downwind distance from the source

with the mean concentration measured in the experiment of Legg et al. (1986) is obtained using the value of T_L reported by the same authors. For this reason the value of C_0 must be selected according to different criteria. We chose the value $C_0 = 2$ (at the lower limit of the commonly accepted values) to obtain a mean dissipation vertical profile (from the relation $\varepsilon = 2\langle u_3^2\rangle / C_0 T_L$) comparable with that obtained using different methods in Raupach et al. (1986). A comparison between different estimates of the mean dissipation is shown in Fig. 6. Due to the smaller value of C_0 used here with respect to the value used in Cassiani et al. (2005a) a proportionally smaller value of C_r must be used; a direct proportionality between the value of C_0 and C_r has been recently shown in Franzese and Cassiani (2006).

5.1 Discussion of model results

An important parameter in the definition of the concentration fluctuations is the source size σ_0 (see e.g., Thomson 1990); $\sigma_0 = 4.5$ mm has been chosen here to ensure agreement between the measured and modelled absolute spread close to the source in the single-line source experiment.

The vertical spread (σ_z) computed by the model for two different source sizes is shown in Fig. 7; the smaller source size ($\sigma_0 = 0.9$ mm) is the wire diameter and the larger source ($\sigma_0 = 4.5$ mm) has been selected to better fit the measurements

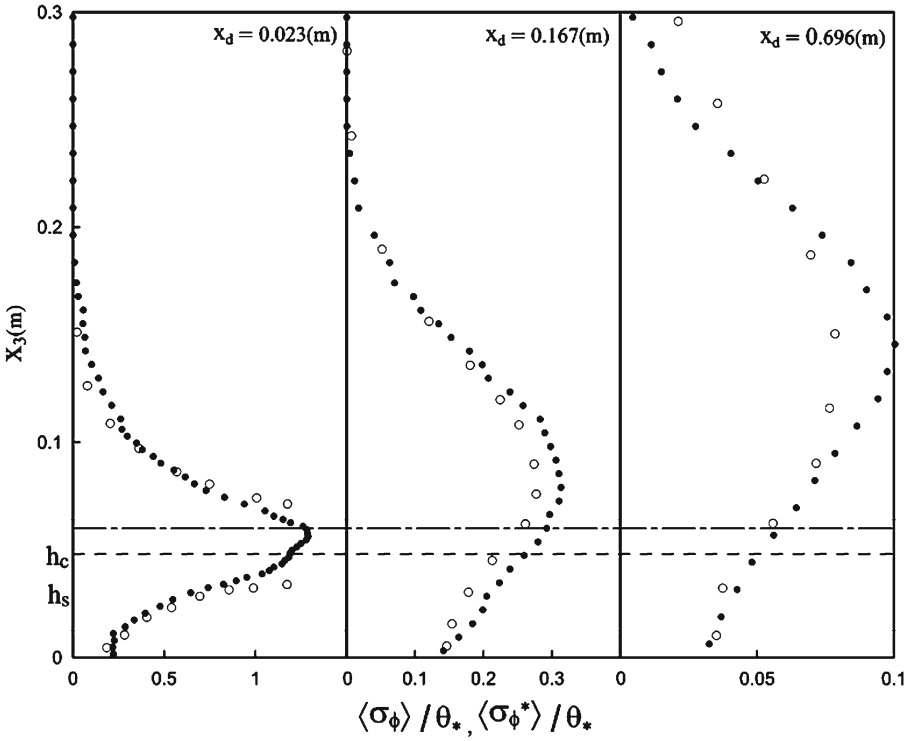

Fig. 10 Measured (σ_ϕ, ○) and modelled (σ_{ϕ^*}, •) temperature standard deviation normalized with the temperature scale θ_* (see Table 1). Single-line source experiments of Legg et al. (1986). $h_c = 0.06$ m is the canopy height; $h_s = 0.048$ m is the source height; x_d is the downwind distance from the source

of Legg et al. (1986). This size is larger than the effective wire diameter used in the single-line source and multiple-line source experiments, respectively, and suggests that the behaviour around the source cannot be modelled in a simple manner and this may also be related with the upwind dispersion as discussed in Legg et al. (1986). Choosing the source size to ensure good agreement with the absolute spread close to the source is perhaps the simplest way to parameterize these effects. This introduces a degree of arbitrariness in the comparison since the concentration fluctuations are influenced by the source size.

In the definition of the micromixing time scale the parameter $\gamma = 0.82$ has been chosen to ensure overall agreement with the temperature variance profiles measured for the single-line source experiment, and is close to the value used in Cassiani et al. (2005a) for a neutral boundary layer. However, this agreement could be fortuitous since it is influenced by the choice of the source size. For example, similar results could be obtained using the smaller source size but a different value for the empirical parameter $\gamma = 0.3$–0.4.

The micromixing time scale (t_m) resulting for single-line source and multiple-line sources are shown in Fig. 8a and 8b, respectively, with values defined for the fraction of the domain covered by the absolute (mean) spread according to Eq. 23. Outside of this region we used the equilibrium relation as explained above. It can be seen that in

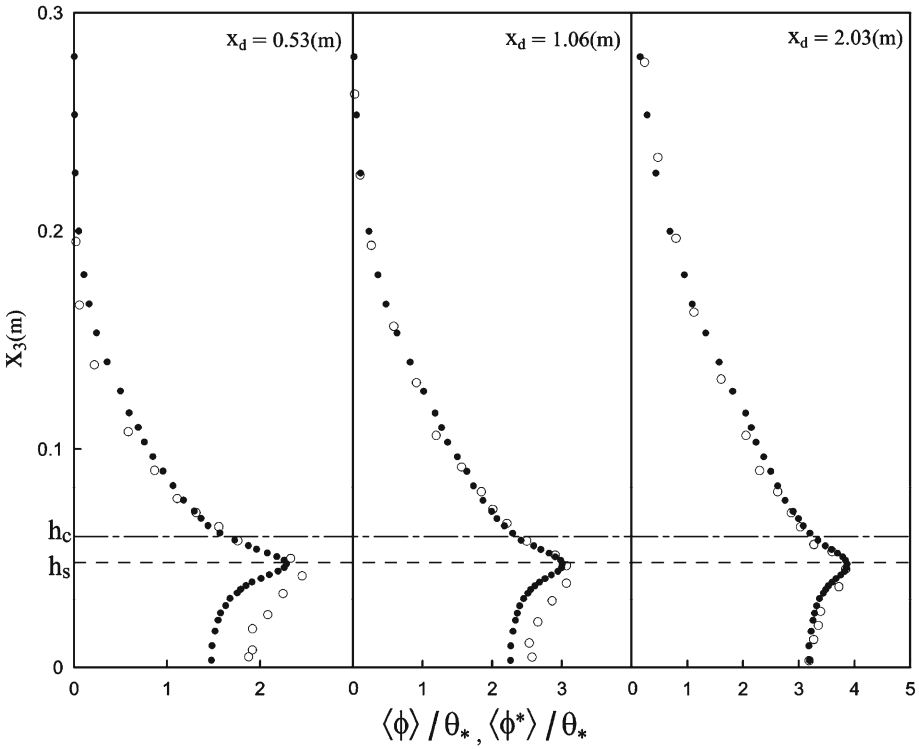

Fig. 11 Measured ($\langle\phi\rangle$, ○) and modelled ($\langle\phi^*\rangle$, •) mean temperature normalized with the temperature scale θ_* (see Table 1). Multiple-line source experiments of Coppin et al. (1986). $h_c = 0.06$ m is the canopy height; $h_s = 0.051$ m is the source height; x_d is the downwind distance from the first source

both cases the time scale grows with the distance from the source, where the minimum local value is around the source height release, with a local peak close the ground. The general behaviour is growth with elevation above the ground although a local peak can be seen at intermediate elevations relative to the plume vertical spread. The effect of a series of sources is to shorten the time scale but not upwind to the first source. Here, in contrast, the time scale is slightly larger and this is due to the upwind transport. It can be seen that the time scale becomes small close to every source. At the same time we observe that the time scale increases more rapidly for the sources at a greater downwind distance from the first source.

The normalized mean temperature vertical profile obtained by our model for the single source simulation is shown in Fig. 9, together with that for the experiments of Legg et al. (1986); x_d is the downwind distance from the source, where three downwind distances are shown. The agreement can be considered good for all distances, as is to be expected for this class of models. The single source measured, normalized, temperature standard deviation $\sigma_\phi = \left\langle(\phi - \langle\phi\rangle)^2\right\rangle^{1/2}$, together with that obtained by our model, are shown in Fig. 10. The agreement can be considered good for all the distances. In the first measured profile, $x_d = 0.023$ m, the peak is not shown due its absence in the measurements reported in Legg et al. (1986), however it seems to be an underestimation in the model prediction. It can be appreciated that the model is

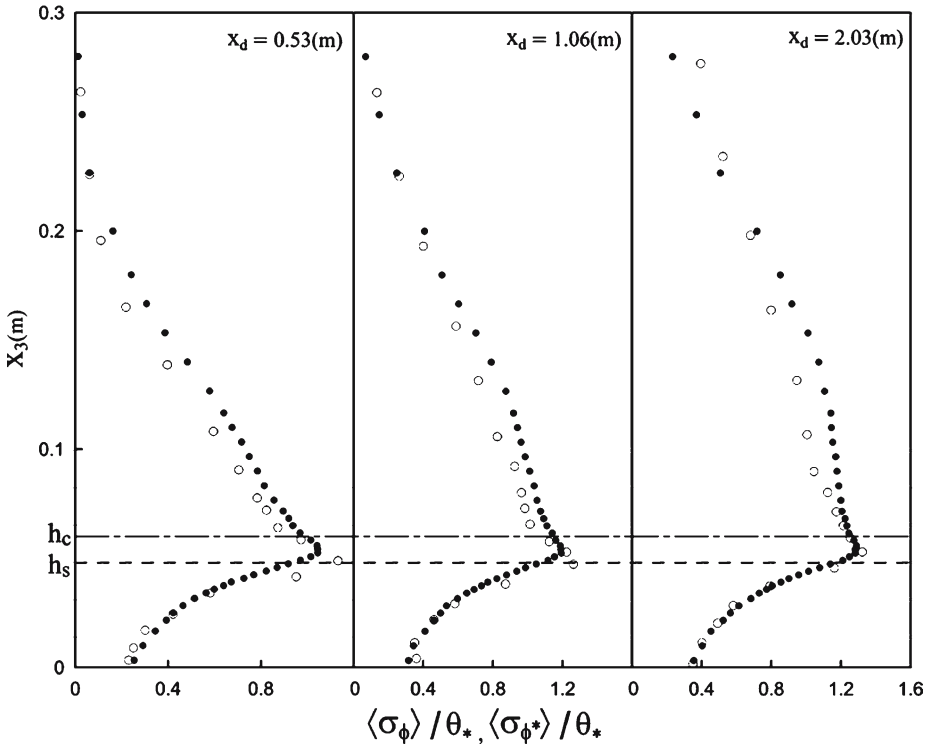

Fig. 12 Measured (σ_ϕ, ○) and modelled (σ_{ϕ^*}, ●) temperature standard deviation normalized with the temperature scale θ_* (see Table 1). Multiple-line source experiments of Coppin et al. (1986). $h_c = 0.06$ m is the canopy height; $h_s = 0.051$ m is the source height; x_d is the downwind distance from the first source

able to correctly reproduce the elevation of the peak above the ground. These results show that the parameterization for t_m and the extensions to inhomogeneous conditions, including the wind-shear effect, is effective. Moreover, the good resolution of the peak shows that the use of the nested grid approach is able to correctly resolve the concentration field.

The normalized modelled temperature mean and standard deviation for multiple-line sources are shown in Figs. 11 and 12, respectively, together with the measurements reported in Coppin et al. (1986); here x_d is the downwind distance from the first line source. The overall source power $Q_s = 275\,\mathrm{W\,m^{-2}}$ was converted to an individual source power of $Q_s = 6.1\,\mathrm{W\,m^{-1}}$, considering approximately 45 sources $\mathrm{m^{-1}}$, and based on the data reported in Table 1. As expected for this class of model, the mean concentration is well reproduced. The agreement between measured and modelled profiles of concentration variance is good showing that the simple t_m extension to account for multiple sources is effective and that the block structured grid is able to correctly capture the concentration field.

The multiple source measured and modelled skewness, $S = \left\langle (\phi - \langle\phi\rangle)^3 \right\rangle \left(\sigma_\phi^3\right)^{-1}$ and S^*, are shown in Fig. 13. Overall the agreement is good, but the model seems not to be capable of completely capturing the behaviour close to the source elevation. However, this level of discrepancy between the model and measurements is probably

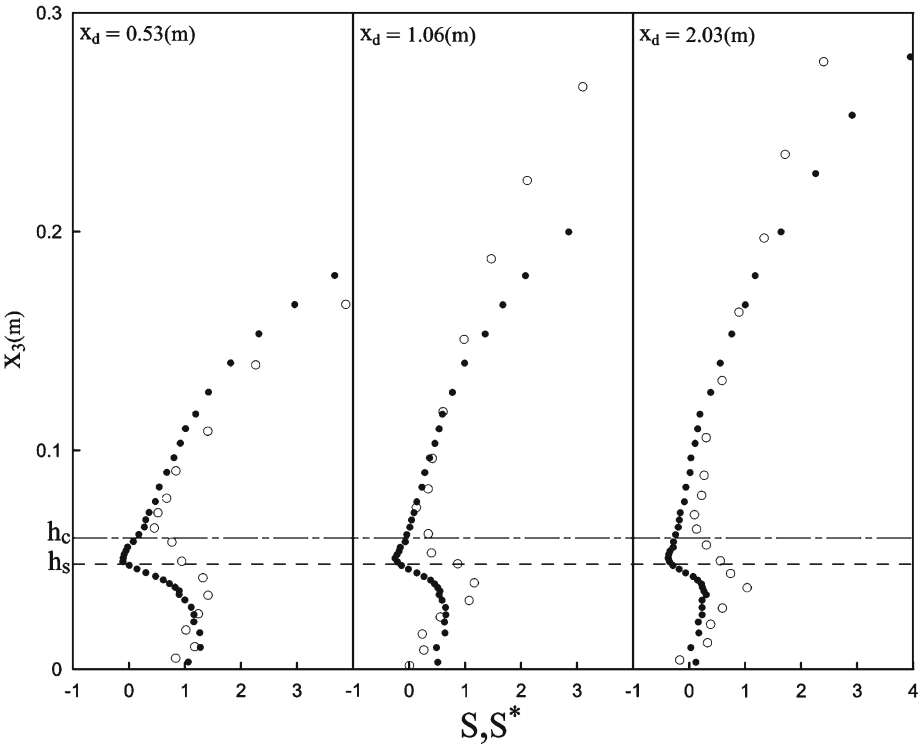

Fig. 13 Measured ($S, \circ$) and modelled ($S^*, \bullet$) temperature skewness. Multiple-line source experiments of Coppin et al. (1986). $h_c = 0.06$ m is the canopy height; $h_s = 0.051$ m is the source height; x_d is the downwind distance from the first source

unavoidable considering the approximation in the model inputs (statistics profile) and the intrinsic limitation of the model itself. The value at the ground is correctly captured. The measured kurtosis, $K = \left\langle \left(\phi - \langle\phi\rangle\right)^4 \right\rangle \left(\sigma_\phi^4\right)^{-1}$, and the modelled one, K^*, are reported in Fig. 14. Again, the overall agreement is good although the model is incapable of predicting the local behaviour at the source elevation.

The third- and fourth-order moments are shown in Fig. 15 for the last measurement position $x_d = 2.03$. We include these comparisons since these moments are actually the most significant for characterizing chemical reactions, i.e. chemical reactions are functions of the concentration not of the normalized fluctuations of concentration. It can be seen that the model is able to correctly reproduce these higher moments of concentration.

The modelled cumulative distribution functions (CDFs) for the single-source release at two elevations above the ground and several downwind distances are shown in Fig. 16. The simulated CDF evolves from that related to an exponential-like pdf to a Gaussian-like form. These results show the model's potential for predicting all the one-point statistics, and when complete measurements are lacking could be used as a useful comparison for other modelling approaches such as large-eddy simulation.

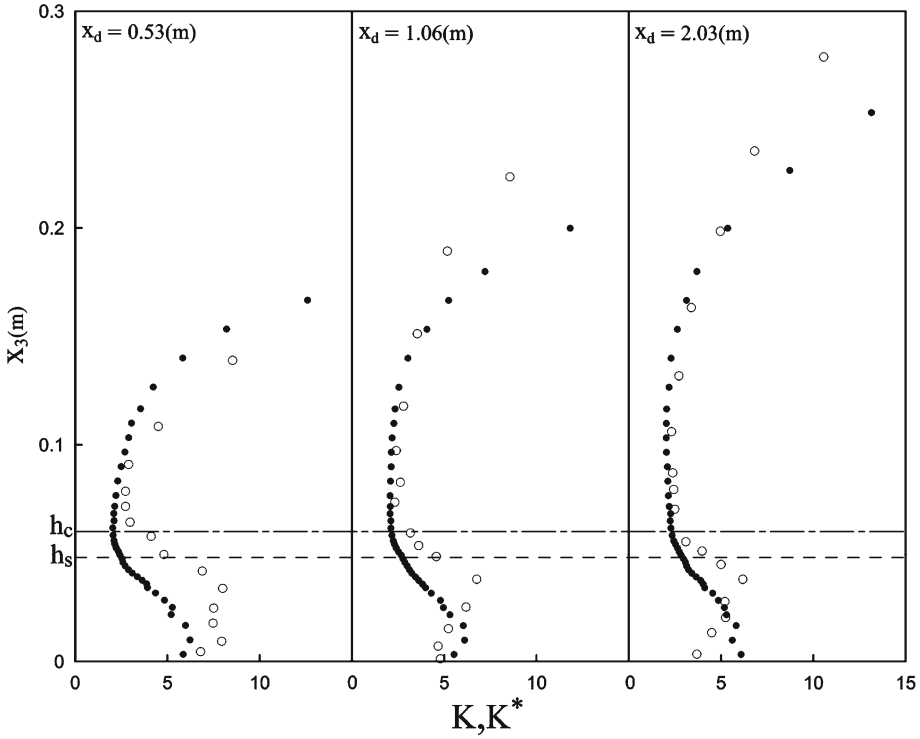

Fig. 14 Measured ($K, \circ$) and modelled ($K^*, \bullet$) temperature kurtosis. Multiple-line source experiments of Coppin et al. (1986). $h_c = 0.06$ m is the canopy height; $h_s = 0.051$ m is the source height; x_d is the downwind distance from the first source

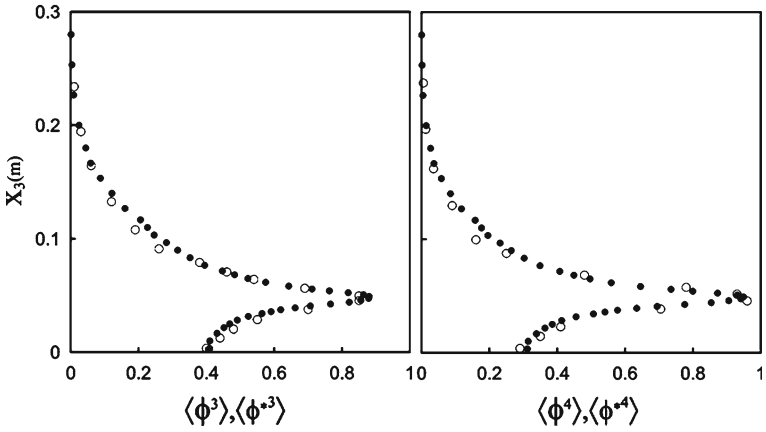

Fig. 15 Measured ($\circ$) and modelled ($\bullet$) third ($\langle\phi^3\rangle, \langle\phi^{*3}\rangle$) and fourth ($\langle\phi^4\rangle, \langle\phi^{*4}\rangle$) moments of temperature. Multiple-line source experiments of Coppin et al. (1986). The downwind distance from the first source is $x_d = 2.03$ m

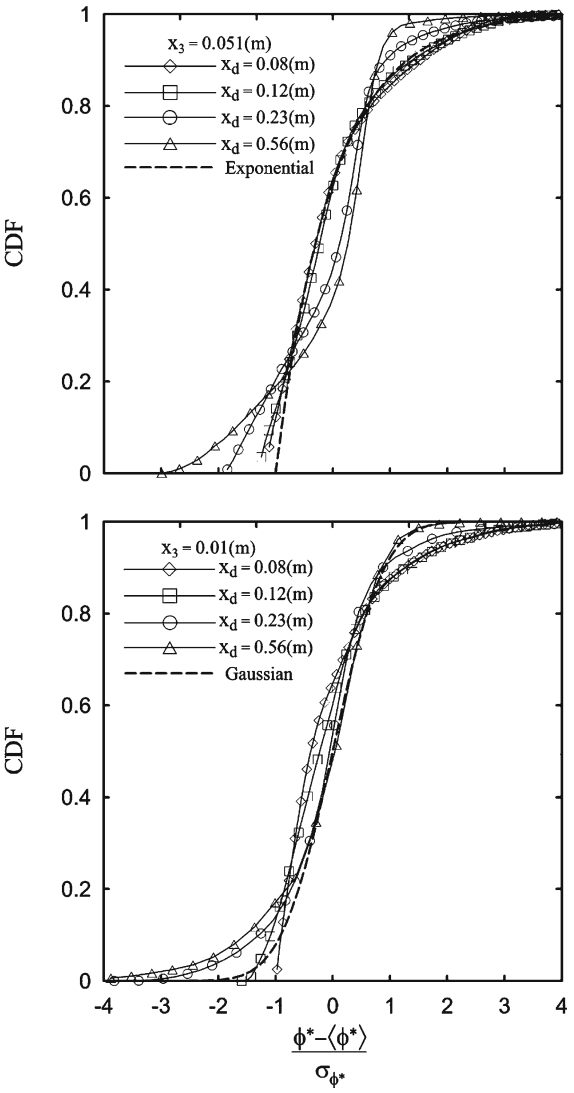

Fig. 16 Modelled cumulative distribution function (CDF) for the single-line source experiment; sampling at the source elevation ($x_3 = 0.051$ m) and close to the ground ($x_3 = 0.01$ m) at four different downwind distances. The Gaussian and exponential CDF with zero mean and unit variance are given for reference

6 Conclusion

A model based on the Lagrangian stochastic particle approach coupled with an IECM micromixing model has been presented. The model is capable of computing the mean and fluctuating fields from single- and multiple-line sources in a canopy layer and includes the effects of wind shear and along-wind turbulence.

A model for the micromixing time scale (t_m) needed in the IECM model has been presented, extending that proposed in Cassiani et al. (2005a), including a mean shear effect, along-wind turbulence and multiple sources. The results obtained by the model are promising but the dependence of the results on the values of several constants

(C_0, C_r, C_ϕ), and on the choice of the scalar source size, requires further comparisons with experiments to fully validate the model's generality.

A Monte Carlo algorithm has been developed based on the concept of a block-structured grid and particle splitting and erasing. This algorithm is able to efficiently account for small sources and can be easily adapted to complex geometry thus allowing the application of the proposed model to cases of practical interest.

The inclusion of a simple chemical reaction involving few chemical species is straightforward and is under investigation while the treatment of complex atmospheric chemistry in the modelling is a formidable computational challenge. However, it is possible to show that the intrinsic dimension of a typical tropospheric chemical model is low (Lowe and Tomlin 2000) and therefore by using a lower-dimensional representation of the chemistry, saving can be made in terms of the number of equations in the chemical model. Thus future development of the proposed approach will allow the use of pdf Monte Carlo methods even for complex atmospheric chemistry.

Acknowledgements We acknowledge an anonymous reviewer for helpful comments. M. Cassiani and J. Albertson were supported by the office of Science (BER), US Department of Energy, and through the Southeast Regional Center of the National Institute for Global Environmental Change under Cooperative Agreement No. DE-FC02-03ER63613.

Appendix

The equations for the drift coefficient a_i are,

$$a_1 = -\frac{1}{2\left\langle u_1^2\right\rangle\left\langle u_3^2\right\rangle - \langle u_1 u_3\rangle^2} b_{11}^2 \left(\left\langle u_3^2\right\rangle u_1^* - \langle u_1 u_3\rangle u_3^*\right) + \frac{\Phi_1}{f_u^*}, \tag{24}$$

$$a_3 = -\frac{1}{2\left\langle u_1^2\right\rangle\left\langle u_3^2\right\rangle - \langle u_1 u_3\rangle^2} b_{33}^2 \left(\left\langle u_1^2\right\rangle u_3^* - \langle u_1 u_3\rangle u_1^*\right) + \frac{\Phi_3}{f_u^*}, \tag{25}$$

$$a_2 = -\frac{1}{2} b_{22}^2 \left\langle u_2^2\right\rangle^{-1} u_2^* + \frac{\Phi_2}{f_u^*} \tag{26}$$

with

$$\begin{aligned}\frac{\Phi_1}{f_u^*} = {} & \frac{1}{2}\frac{\partial\langle u_1 u_3\rangle}{\partial x_3} + \left(\frac{1}{2\left\langle u_1^2\right\rangle\left\langle u_3^2\right\rangle - \langle u_1 u_3\rangle^2}\right) \\ & \times \left[u_1^* u_3^* \left(\left\langle u_3^2\right\rangle \frac{\partial\left\langle u_1^2\right\rangle}{\partial x_3} - \langle u_1 u_3\rangle \frac{\partial\langle u_1 u_3\rangle}{\partial x_3}\right)\right. \\ & \left. + u_3^* u_3^* \left(\left\langle u_1^2\right\rangle \frac{\partial\langle u_1 u_3\rangle}{\partial x_3} - \langle u_1 u_3\rangle \frac{\partial\left\langle u_1^2\right\rangle}{\partial x_3}\right)\right],\end{aligned} \tag{27}$$

$$\frac{\Phi_3}{f_u^*} = \frac{1}{2}\frac{\partial\left\langle u_3^2\right\rangle}{\partial x_3} + \left(\frac{1}{2\left\langle u_1^2\right\rangle\left\langle u_3^2\right\rangle - \langle u_1 u_3\rangle^2}\right) \times \left[u_1^* u_3^* \left(\left\langle u_3^2\right\rangle \frac{\partial\langle u_1 u_3\rangle}{\partial x_3} - \langle u_1 u_3\rangle \frac{\partial\left\langle u_3^2\right\rangle}{\partial x_3}\right) + u_3^* u_3^* \left(\left\langle u_1^2\right\rangle \frac{\partial\left\langle u_3^2\right\rangle}{\partial x_3} - \langle u_1 u_3\rangle \frac{\partial\langle u_1 u_3\rangle}{\partial x_3}\right)\right], \tag{28}$$

$$\frac{\Phi_2}{f_u^*} = u_2^* u_3^* \frac{1}{2\left\langle u_2^2\right\rangle}\frac{\partial\left\langle u_2^2\right\rangle}{\partial x_3}. \tag{29}$$

Each component is evaluated at the particle location.

References

Baldocchi D (1992) A Lagrangian random walk model for simulating water vapour, CO_2 and sensible heat flux densities and scalar profile over and within a soybean canopy. Boundary-Layer Meteorol 61:113–144

Brown RJ, Bilger RW (1998a) Experiments on reacting plume-1. Conventional concentration statistics. Atmos Environ 32(4):611–628

Brown RJ, Bilger RW (1998b) Experiments on reacting plume-2. Conditional concentration statistics. Atmos Environ 32(4):629–646

Brown RJ, Woodfield PL (2004) Prediction of short-range maximum NO_2 concentrations using scalars pdfs. Atmos Environ 38(4):1379–1386

Brunet Y, Finnigan JJ, Raupach MR (1994) A wind tunnel study of air flow in waving wheat: single point velocity statistics. Boundary-Layer Meteorol 70:95–132

Cassiani M, Franzese P, Giostra U (2005a) A PDF micromixing model of dispersion for atmospheric flow Part I: development of the model, application to homogeneous turbulence and to neutral boundary layer. Atmos Environ 39(8):1457–1469

Cassiani M, Franzese P, Giostra U (2005b) A PDF micromixing model of dispersion for atmospheric flow. Part II: application to convective boundary layer. Atmos Environ 39(8):1471–1479

Cassiani M, Radicchi A, Giostra U (2005c) Probability density function modelling of concentration fluctuation in and above a canopy layer Agric For Meteorol 133:153–165

Cassiani M, Radicchi A, Albertson JD, Giostra U (2006) An efficient algorithm for scalar pdf modelling in incompressible turbulent flow; numerical analysis with evaluation of IEM and IECM micromixing models. J Comput Phys, in press

Coppin PA, Raupach MR, Legg BJ (1986) Experiments on scalar dispersion within a model plant canopy. Part II: an elevated plane source. Boundary-Layer Meteorol 35:167–191

Dopazo C, O'Brien EE (1974) An approach to the auto ignition of a turbulent mixture. Acta Astronaut 1:1239–1266

Dopazo C, Valino L, Fuego F (1997) Statistical description of the turbulent mixing of scalar fields. Int J Mod Phys B 11(25):2975–3014

Du SM, Sawford BL, Wilson JD, Wilson DJ (1995) Estimation of the Kolmogorov constant (C-0) for the Lagrangian Structure Function, using 2nd-order Lagrangian model of grid turbulence. Phys. Fluids 7(12):3083–3090

Du S (1997) Universality of the Lagrangian structure function constant (C_0) across different kinds of turbulence. Boundary-Layer Meteorol 83:207–219

Fackrell JE, Robins AG (1982) Concentration fluctuations and fluxes in plumes from point sources in turbulent boundary layer. J Fluid Mech 117:1–26

Franzese P (2003) Lagrangian stochastic modelling of a fluctuating plume in the convective boundary layer. Atmos Environ 37:1691–1701

Franzese P, Cassiani M (2006) A statistical Theory of turbulent relative dispersion. J Fluid Mech In Press

Flesch TK, Wilson JD (1992) A two dimensional trajectory simulation model for non Gaussian inhomogeneous turbulence within plant canopies. Boundary-Layer Meteorol 61:349–374

Fox RO (1996) On velocity conditioned scalar mixing in homogeneous turbulence. Phys Fluids 8:2678–2691
Fox RO (2003) Computational models for turbulent reacting flows. Cambridge University Press, Cambridge, 419 pp
Gardiner CW (1983) Handbook of stochastic methods for physics chemistry and the natural sciences. Springer-Verlag, Berlin 442 pp
Garmory A, Richardson ES, Mastorakos E (2006) Micromixing effects in a reacting plume by the stochastic fields method. Atmos Environ 40:1078–1091
Gifford FA (1977) Tropospheric relative diffusion observations. J Appl Meteorol 16:311–313
Griffith RF, Megson LC (1984) The effect of uncertainties in human toxic response on hazard range estimation for ammonia and chlorine. Atmos Environ 18:1195–1206
Heinz S (2003) Statistical mechanics of turbulent flows. Springer Verlag, Berlin Heidelberg, 214 pp
Hilderman TL, Hrudey SE, Wilson DJ (1999) A model for effective toxic load from fluctuating gas concentrations. J Hazard Mater A 64:115–134
Jenny P, Pope SB, Muradoglu M, Caughey DA (2001) A hybrid algorithm for the joint pdf equation of turbulent reactive flows. J Comput Phys 166:218–252
Legg BJ, Raupach MR, Coppin PA (1986) Experiments on scalar dispersion within a model plant canopy. Part III: an elevated line source. Boundary-Layer Meteorol 35:277–302
Li G, Modest MF (2001) An effective particle tracking scheme on structured/unstructured grids in hybrid finite volume/pdf Monte Carlo methods. J Comput Phys 173:187–201
Lien RC, D'Asaro E (2002) The Kolmogorov constant for the Lagrangian velocity spectrum and structure function. Phys Fluids 14:4456–4459
Lowe R, Tomlin A (2000) Low-dimensional manifolds and reduced chemical models for tropospheric chemistry simulations. Atmos Environ 34:2425–2436
Luhar AK, Sawford BL (2005a) Micromixing modelling of concentration fluctuations in inhomogeneous turbulence in the convective boundary layer. Boundary-Layer Meteorol 114:1–30
Luhar AK, Sawford BL (2005b) Micromixing modelling of mean and fluctuating scalar fields in the convective boundary layer. Atmos Environ 39:6673–6685
Monin AS, Yaglom AM (1975) Statistical fluid mechanics, Vol. 2. MIT Press, Cambridge, MA, 874 pp
Meeder JP, Nieuwstadt FTM (2000) Large eddy simulation of the turbulent dispersion of a reactive plume from point source into a neutral atmospheric boundary layer. Atmos Environ 34:3563–3573
Patton EG, Kenneth JD, Barth MC, Sullivan PP (2001) Decaying scalar emitted by a forest canopy: a numerical study. Boundary-Layer Meteorol 100:91–129
Poggi D, Katul G, Albertson J (2006) Scalar dispersion within model canopy: measurement and three-dimensional Lagrangian models. Adv Water Resour 29:326–335
Pope SB (1985) Pdf methods for turbulent reactive flows. Prog Energy Combust Sci 11:119–192
Pope SB (1994) Lagrangian pdf methods for turbulent flows. Annu Rev Fluid Mech 26:23–63
Pope SB (1998) The vanishing effect of molecular diffusivity on turbulent dispersion: implications for turbulent mixing and the scalar flux. J Fluid Mech 359:299–312
Pope SB (2000) Turbulent flows. Cambridge University Press, Cambridge, 806 pp
Raupach MR, Coppin PA, Legg BJ (1986) Experiments on scalar dispersion within a model plant canopy. Part I: the turbulence structure. Boundary-Layer Meteorol 35:21–52
Raupach MR, Coppin PA, Legg BJ (1987) Erratum to Raupach MR, Coppin PA, Legg BJ, 1986. Experiments on scalar dispersion within a model plant canopy. Part I: the turbulence structure. Boundary-Layer Meteorol 35:21–52. Boundary-Layer Meteorol 39:423–424
Raupach MR, Finnigan JJ, Brunet Y (1996) Coherent eddies and turbulence in vegetation canopies: the mixing-layer analogy. Boundary-Layer Meteorol 78:351–382
Reynolds AM (1998) Comments on the 'Universality of the Lagrangian velocity structure function constant (C-0) across different kinds of turbulence'. Boundary-Layer Meteorol 89:161–170
Rodean HC (1996) Stochastic Lagrangian models of turbulent diffusion. Am Meteorol Soc, Met. Monogr 26(48):82 pp
Sawford BL (1999) Rotation of trajectories in Lagrangian stochastic models of turbulent dispersion. Boundary-Layer Meteorol 93:411–424
Sawford BL (2004) Micro-mixing modelling of scalar fluctuations for plumes in homogeneous turbulence. Flow Turb Combust 72:133–160
Sawford BL (2006) Lagrangian stochastic modelling of chemical reaction in a scalar mixing layer. Boundary-Layer Meteorol 118:1–23

Subramaniam S, Pope SB (1998) A mixing model for turbulent reactive flows based on Euclidean minimum spanning trees. Combust Flame 115:487–514
Thomson DJ (1987) Criteria for the selection of the stochastic models of particle trajectories in turbulent flows. J Fluid Mech 180:529–556
Thomson DJ (1990) A stochastic model for the motion of particle pairs in isotropic high-Reynolds-number turbulence, and its application to the problem of concentration variance. J Fluid Mech 210:113–153
Vickers NJ, Christensen TA, Baker TC, Hildebrand JG (2001) Odour-plume dynamics influence the brain's olfactory code. Nature 410:466–470
Vilà-Guerau de Arellano J, Dosio A, Vinuesa J-F, Holtslag AAM, Galmarini S (2004) The dispersion of chemically reactive species in the atmospheric boundary layer. Meteorol Atmos Phys 87:23–38
Wilson DJ (1995) Concentration fluctuations and averaging time in vapor clouds. Center for Chemical Process Safety, American Institute of Chemical Engineers, New York, 181 pp
Wilson JD, Flesch TK (1997) Trajectory curvature as a selection criterion for valid Lagrangian stochastic dispersions models. Boundary-Layer Meteorol 84:411–426
Yee E (2001) An analytical model for threshold crossing tares of concentration fluctuations in dispersing plumes. Boundary-Layer Meteorol 98:517–527